Environmental Science Processes & Impacts

ROYAL SOCIETY OF CHEMISTRY

PAPER

Check for updates

Cite this: *Environ. Sci.: Processes Impacts*, 2022, **24**, 2419

Dissolution of Mn-bearing dolomite drives elevated Cr(VI) occurrence in a Permian redbed aquifer†

Jeffrey P. Westrop,‡[a] Zachary D. Tomlinson,[a] Brandon M. Maples,[a] Kato T. Dee,[a] Andrew L. Swindle,[b] Megan E. Elwood Madden,[a] Qinhong Hu[c] and Andrew S. Elwood Madden*[a]

Municipalities in central Oklahoma, U.S.A. increasingly rely on water drawn from the Central Oklahoma Aquifer (COA) as surface water resources have not grown in proportion to population and current water demands. However, water drawn from certain regions of the COA frequently contains elevated levels of naturally occurring hexavalent chromium. Rock samples from the Norman Arsenic Test Hole Core (NATHC) were investigated to identify the mineralogic host(s) of Cr and mechanisms of Cr(VI) release *via* bulk mineralogy and chemistry measurements, selective chemical extractions, and microscale elemental analyses. Results demonstrate most COA Cr is contained in Fe oxides and clays as isomorphic substitutions for Fe(III). Analyses of regional groundwater data, including hierarchical clustering methods and GIS, demonstrate the most intense Cr(VI) occurrence is linked to cation exchange with Na-clays at depth. Cation exchange allows dissolution of Mn-bearing dolomite, which in turn produces Mn oxides in otherwise dolomite-saturated groundwaters. Mn oxides in turn are known to oxidize Cr(III) to Cr(VI). In general, co-occurrence of Mn-bearing carbonates and exchangeable clays in any aquifer, particularly those with Cr(III) present in iron oxide cements, serve as ingredients for groundwater occurrences of oxidizable trace metals.

Received 27th September 2022
Accepted 8th November 2022

DOI: 10.1039/d2em00395c

rsc.li/espi

Environmental significance

Geogenic groundwater occurrences of toxic hexavalent chromium Cr(VI) typically involve oxidation of Cr(III) to Cr(VI), typically associated with ultramafic rocks. However, a Permian redbed clastic aquifer in Central Oklahoma, U.S.A. experiences naturally occurring groundwater chromium concentrations exceeding 100 ppb. Understanding the processes underpinning Cr(VI) mobilization is integral for communities that rely on these aquifers for drinking water. The link between Cr(III) oxidation and manganese(III/IV) oxides is well established. Our study demonstrates that not only can redbed aquifers contain environmentally significant concentrations of Cr(III) substituted in Fe(III) oxides, the co-location of Mn-bearing carbonates and exchangeable clay minerals leads to enhanced groundwater Cr occurrence. We link Cr occurrence to oxidation of Mn(II) released from cation-exchange enhanced carbonate dissolution driving Cr(III) oxidation.

Introduction

Hexavalent chromium (Cr(VI)) contamination of surface and groundwater remains a well-known and widespread problem, affecting hundreds of sites within the United States alone,[1] leading to continued development of remediation methods for active or passive treatment of Cr(VI)-contaminated groundwater.[2–8] Although Cr(VI) typically occurs only as a trace constituent in many natural uncontaminated systems, Cr(III) is common in rocks, minerals, and soils as a chemical analog to Fe(III).[9] In the United States, recent re-evaluations of Cr(VI) toxicity through drinking water ingestion[10] have led to increased scrutiny of Cr(VI) concentrations in drinking water, resulting in new proposed health goals and possible new U.S. E.P.A. Cr(VI) rules.[11] Therefore, a mechanistic understanding about how Cr(III) oxidizes and Cr(VI) accumulates in natural aquifer systems is required for many communities to address this increased focus on Cr(VI) toxicity.

Sorption/desorption of Cr(VI) and oxidation/reduction of Cr are key processes controlling Cr cycling in both contaminated and natural environments.[12,13] The chromate anion predominantly sorbs to common aquifer minerals with positive surface charges such as Fe-oxides and clay edges, leading to a strong pH-dependence; Cr(VI) desorbs at high pH as mineral surface

[a]*University of Oklahoma, School of Geosciences, 100 E. Boyd St., Norman, OK 73069, USA. E-mail: amadden@ou.edu*

[b]*Wichita State University, 1845 Fairmount Avenue, Wichita, Kansas 67260, USA*

[c]*University of Texas at Arlington, 500 Yates Street, Arlington, TX 76019, USA*

† Electronic supplementary information (ESI) available: Additional details on methods, detailed results of bulk chemistry and mineralogy by powder X-ray diffraction, SEM imaging, microprobe and LA-ICP-MS data, and groundwater data analysis are presented, along with a csv file containing groundwater data used in statistical analyses. See DOI: https://doi.org/10.1039/d2em00395c

‡ Present address: University of Nebraska-Lincoln, Nebraska Conservation and Survey Division, School of Natural Resources, 612 Hardin Hall, Lincoln, Nebraska, 68588, USA

functional groups deprotonate.[14,15] Oxidation/reduction reactions involving Cr(III) critically control Cr(VI) availability to human exposure.[16] Millions of people eat every day with stainless steel utensils made from several to tens of percent Cr protected by a Cr(III)-film; however, the extremely slow reaction of Cr(III) with oxygen alleviates concerns about generating Cr(VI). In natural systems, Cr(III) oxidation is thought to occur predominantly through contact with Mn(III/IV)-oxides.[17–23] Laboratory experiments demonstrate that Cr(III) reacts with Mn oxides *via* a surface complex, most rapidly at acidic pH.[24–38] Despite slower kinetics and experimental challenges due to the low solubility of Cr or mixed Cr–Fe hydroxides, laboratory[20,33,39–41] and field[23,42] studies indicate that Cr(III) oxidation by Mn oxides is also common in natural systems at neutral to basic conditions.

While research conducted on soils has been useful in identifying specific processes associated with Cr mobility into shallow groundwater, fewer studies have investigated Cr occurrences in older, deep aquifer sediments.[43] This study combines analyses of sediment cores and geochemical modeling of groundwater chemical data from the Central Oklahoma Aquifer (COA) to increase our understanding of mechanisms by which naturally-occurring Cr(III) hosted in aquifer sediments is oxidized and released as Cr(VI) into groundwater. The COA is a Permian redbed aquifer that serves as a primary source of agricultural, industrial, and municipal water in central Oklahoma, in which the clastic Permian Garber and Wellington Formations are the major water-producers.[43,44] However, water from the COA frequently contains elevated levels of naturally-sourced toxic elements, notably arsenic and hexavalent chromium. Previous research, including investigations of depth-dependent water chemistry at the U.S. Geological Survey/U.S. E.P.A. Norman Arsenic Test Hole (NATH) suggests As release occurs dominantly through desorption from the surfaces of iron oxides within the COA.[43,44] However, less is known regarding the source(s) and mechanism(s) of Cr release into the groundwater, despite higher hexavalent chromium levels in the Oklahoma City region than any other U.S. city municipal water supply tested in a national survey.[45]

Geologic setting

The COA underlies an area of approximately 8000 km^2 of central Oklahoma.[46,47] COA aquifer rocks consist of sandstone interbedded with siltstone, mudstone, and minor thin conglomerate beds.[44,47] Sandstones are dominated by quartz and cemented either by dolomite or a very fine-grained clay mineral/iron oxide matrix, while mudstones are primarily composed of finer-grained quartz plus a greater proportion of clay minerals.[44,48] Conglomerates consist of dolostone clasts in an iron oxide and clay mineral matrix.[48,49] Ubiquitous iron oxides, including hematite and goethite, form cements and coatings on primary grains in sandstones, mudstones, and conglomerates, which give the rocks their characteristic red color. Trace Mn oxides form dendritic cements between quartz grains in both sandstones and mudstones.[44,48]

COA sediments deposited in what is typically described as a fluvial-deltaic environment, associated with in rapid lateral and vertical variations in lithology and groundwater chemistry over short distances.[44,46,47] However, regional trends are evident. Water quality issues are most pronounced in the western third of the COA, where the Permian aquifer units are buried beneath the fine-grained Permian Hennessey Formation (*i.e.*, the "confined" portion of the aquifer). In the eastern two thirds of the COA, the aquifer units are exposed at the surface (*i.e.*, the "unconfined" portion of the aquifer). The COA is typically oxic with dissolved oxygen concentrations greater than 1 ppm; the persistence of oxic conditions can be related to a general lack of organic matter in COA sediments.[44,46,47] Bleached spots within cores and outcrops lack ferric iron oxide grain coatings and are thought to represent localized reducing conditions in the aquifer.[47] Relatively young groundwater in the shallow, unconfined portion of the COA (C^{14} ages <10 000 years old, with estimated water ages ranging from a few hundred years to thousands of years depending on flowpath[46]) is characterized by a Ca, Mg–HCO_3 chemistry and near-neutral pH values,[44,46,47] derived from the dissolution of dolomite in the presence of CO_2 from soil gas.[50] However, as recharge water flows deeper through the aquifer to the confined zone (C^{14} ages 10 000–30 000 years old[46]) it transitions to Na–HCO_3 dominated chemistry and pH values increase to a maximum of about 9.5 (Fig. 1).[44,46,47] This decrease in Ca and Mg concentrations and the corresponding increases in pH and Na concentration result from interactions between clays in the aquifer and groundwater as the concentration of exchangeable Na in clay minerals generally increases with depth.[44,48] As groundwater comes into contact with deeper clays, dissolved Ca and Mg are exchanged for interlayer Na.[44,46,47]

Chromium occurrence in the COA

Chromium occurs naturally both in the COA host rock and groundwater. Earlier studies found Cr in the aquifer associated with iron oxide and clay minerals in mudstones with lower permeability that reduce the extent of rock–water interactions and slow the removal of heavy metals, such as chromate.[46,47] Cr occurs naturally in COA groundwater with a wide range of values, from undetectable to ~130 ppb (μg kg^{-1}, 2.5 μM).[45,47]

Previous depth-dependent groundwater sampling in the COA demonstrated that elevated Cr coincided with higher pH, older water with low Ca–Mg and elevated Na (Fig. 1, ESI†).[44] Generally, groundwater pH in the COA correlates with age,[46,47,51] where lower pH corresponds more closely to meteoritic precipitation while pH increases with increasing water-rock contact time. The oxygenated (>1 ppm DO) conditions and low organic matter content in the groundwater indicate that aqueous chromium will be generally stable as oxidized Cr(VI)/chromate. High pH conditions were previously hypothesized to enhance desorption of Cr(VI) from the surfaces of iron oxide minerals and the surfaces and edges of clay minerals, similar to the behavior of arsenic in the COA.[44,46,47] However, adsorbed Cr was not found above the detection limit during sequential extractions of sediment cores,[52] suggesting other release mechanisms are at play. Furthermore, Cr occurrence is highly variable above pH 7, with no clear relationship between pH and

 This journal is © The Royal Society of Chemistry 2022

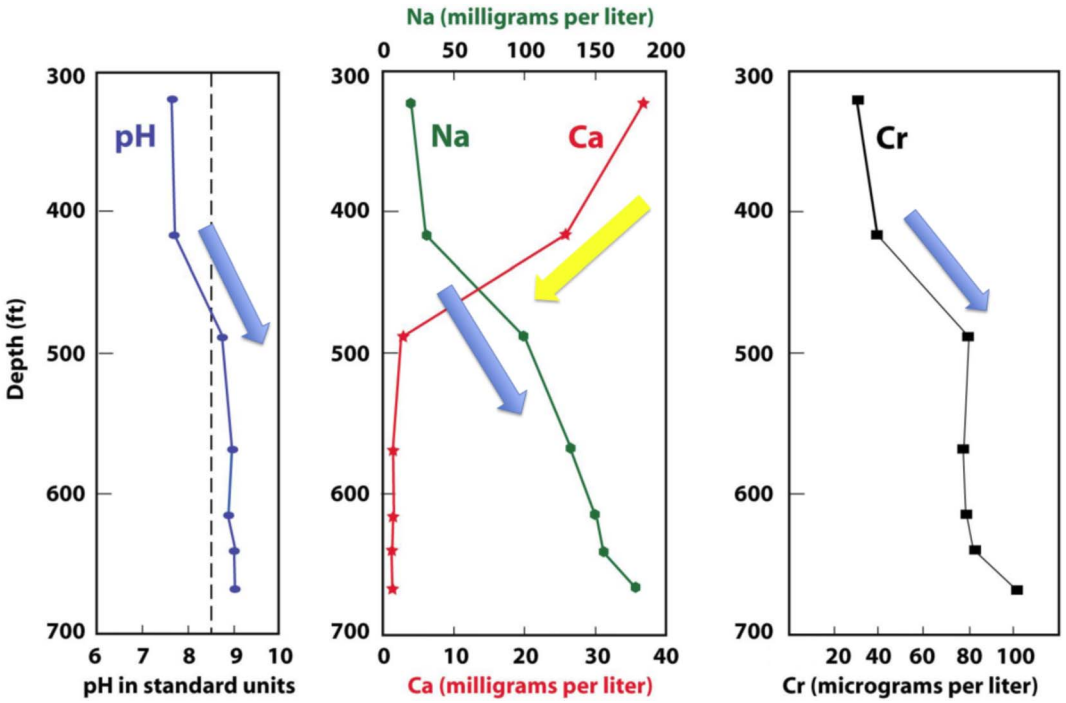

Fig. 1 Depth-dependent water chemistry from the Norman Arsenic Test Hole as determined by, and adapted from, Smith *et al.* (2009). Each dot represents a water chemistry sampled from a depth isolated as close as possible to highly conductive sandy sediment layer. Deeper samples correspond to older groundwaters.

Cr observed. Indeed, both age and pH serve as poor predictors of groundwater Cr in contrast to As.

In this study, we investigated mineralogical hosts of Cr in core samples from the COA, supplementing chemical extractions and bulk quantitative powder X-ray diffraction (XRD) with microscale spatially resolved chemical measurements (electron probe microanalysis (EPMA) and laser-ablation inductively-coupled mass spectrometry (LA-ICP-MS)). We also investigated processes that lead to Cr(VI) mobilization by evaluating chemical extractions, interrogating core samples for Cr-oxidation potential, and evaluating regional groundwater geochemistry *via* hierarchical clustering and geochemical models, with the goal of understanding the distribution of Cr(VI) and the processes that lead to Cr(VI) accumulation in groundwater in order to develop prediction of which factors lead to risk for elevated Cr(VI). We propose that dissolution of Mn-bearing dolomite, driven by cation exchange between Ca/Mg rich groundwater and Na-bearing clays at depth, and subsequent precipitation of Mn-oxides oxidizes sediment Cr(III) to soluble and groundwater-mobile Cr(VI). This research demonstrates the importance of cation-exchange driven carbonate mineral dissolution on groundwater quality and enhances our knowledge of Cr cycling in Permian redbed aquifers.

Materials and methods

Bulk chemistry and mineralogy of the NATHC

Rock samples were obtained from the Norman Arsenic Test Hole Core (NATHC), which was drilled in an area of the COA with known water quality issues as part of a previous joint USGS/EPA study.[47] Fifty samples were obtained at selected intervals from 303 to 651 ft below ground surface (120–198 m) based on visible changes in lithology or diagenetic textures. Powder XRD, SEM, optical microscopy, and bulk chemical analysis by inductively coupled plasma-mass spectrometry (ICP-MS) were performed on these samples to determine the mineralogical hosts of Cr (details in ESI†). Twelve additional core samples were prepared as petrographic thin sections (Texas Petrographics). Microscale spatially-resolved chemical analyses were collected using electron probe microanalysis (EPMA) and laser-ablation (LA)-ICP-MS from a subset of the thin sections.

Chemical extractions

Fourteen of the 50 samples were selected for further wet chemical treatments based on bulk chemical and mineralogical analysis. First, the sediments were evaluated for net chromium oxidation potential[53] using the selective Mn dissolution method of Neaman and others.[54] A sequential extraction procedure consisting of four chemical extractions modified from Asikainen and Nikolaidis[55] were also performed on representative core samples to identify prominent forms of chromium in the COA. These extractions were designed to target Cr associated with the following fractions: (1) easily dissolved (ultrapure water, (UPW)), (2) adsorbed and ligand exchangeable (1 M potassium phosphate monobasic), (3) Mn oxides (0.1 M hydroxylamine hydrochloride (HHCl); poorly crystalline iron oxides were not identified either by our work or previous studies

of COA cores), and (4) iron oxides, carbonates, and clay minerals (6 N hydrochloric acid). Extracts were analyzed for total Cr by flame atomic absorption spectroscopy (AAS) following modifications of EPA method 7196 as described in Swindle *et al.*[56]

Statistical evaluation and geochemical modeling of groundwater data

Measurements of COA groundwater parameters were extracted from the U.S. Geological Survey National Water Information Service (NWIS) for 291 wells. Data analysis, including processing, clustering, and plotting was performed using a combination of R Studio, ArcGIS, and Geochemists Workbench. Detailed methods are described in the ESI,† and a listing of all wells, locations, and parameters used in the study are also provided as ESI.† Thermodynamic geochemical modeling was performed using Geochemist's Workbench using the Lawrence Livermore National Laboratory standard thermodynamic database. We used thermodynamic data for "disordered" dolomite for our saturation index calculations due to the abundance of divalent cations such as Fe(II) and Mn(II) in COA dolomites.

Results and discussion

Sediment Cr dominantly hosted in Fe(III) oxides

Bulk and microscale analyses of core samples provide evidence for Cr in both crystalline iron oxide (predominantly hematite) and clay minerals (see ESI† for expanded results of bulk chemistry, powder XRD, *etc.*), with the greatest abundance in hematite. The bulk total Cr correlates somewhat with both bulk total Fe based on LA-ICP-MS data ($R^2 = 0.64$, Fig. 2A) and % clay minerals determined by XRD ($R^2 = 0.51$, Fig. 2B). The better correlation of Cr with bulk total Fe likely reflects the isomorphous substitution of Cr(III) into both clay minerals and iron oxides that contain Fe(III). Scatter in the Cr *vs.* Fe plot likely reflects the presence of additional Fe(II) in carbonates and micas.

Sequential extractions provide additional support for iron oxide and clay mineral sources (Fig. 4, ESI†). Little to no Cr(VI) was associated with the water soluble fraction (ultrapure water extraction) or found incorporated in Mn-oxides (hydroxylamine extraction) (Fig. 4). The ligand exchangeable fraction (PO_4) did contain a small but detectable amount (typically <50 ppb, mean of 45 ppb, range from 22 ppb to 59 ppb) while >500 ppb was typically extracted with 6 N HCl, designed to target iron oxides and clay minerals (mean of 663 ppb, range from 22 to 2031). These results match findings from previous sequential extractions from COA cores collected at generally shallower depths, which also demonstrated that a vast majority of Cr in the COA is locked in crystalline iron oxides and clays as isomorphic substitutions for Fe(III); in those studies, ligand exchangeable Cr was below the detection limit (5 mg Cr per kg rock). We were able to detect the small amounts of ligand-exchangeable Cr with our lower detection limit (~1 ppb in the extract solution).[51] The sample with the smallest HCl-extracted Cr was from 420 ft and was dolomite-bearing.

Microscale analyses provided additional evidence that Cr(III)–Fe(III) isomorphic substitutions provide the dominant source of bulk rock Cr. LA-ICP-MS analyses of dolomitic thin section 473 (depth of 473 ft in the NATH) demonstrated two distinct trends in Fe *vs.* Cr and Al *vs.* Cr (Fig. 6A) concentrations. Since the grain sizes of iron oxides and clays observed by SEM analyses (1–10 μm) (Fig. 3) were much less than the spot size of the LA-ICP-MS (100 μm), each trend can be considered a mixing line reflecting the relative abundance of one mineral phase with a set Al : Fe : Cr stoichiometry within a matrix of other minerals. For example, the high-Fe/low-Al trend (Fig. 6A) with a smaller number of points reflects a less abundant Fe-oxide phase and the low-Fe/high-Al trend reflects a greater volume abundance of clay in most spots within the dolomitic sample. Cr(III) behavior is nearly identical to that of Fe(III), reflecting its incorporation in both iron oxide and clay minerals, with much higher values in the high-Fe (Fe-oxide phase). Analyses of sandstone thin

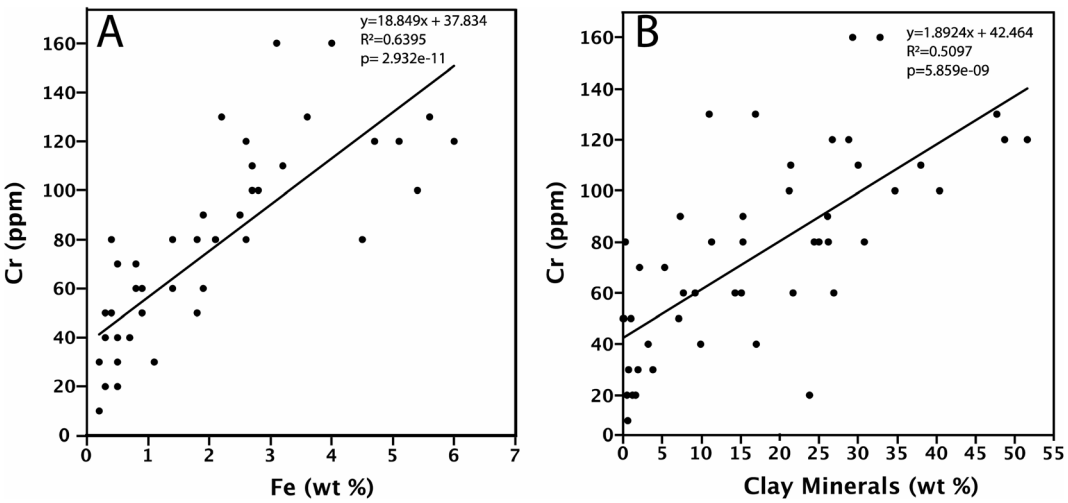

Fig. 2 Whole-rock bulk Cr *vs.* % Fe (A) and Cr *vs.* % clay minerals (B) for the samples obtained from NATH core. Percentage clay was determined by powder XRD; Fe and Cr concentration were determined by ICP-MS. Linear trend lines represent least-squares correlation coefficients but do not imply unique mechanisms; logarithmic fits have similar R^2 values.

 This journal is © The Royal Society of Chemistry 2022

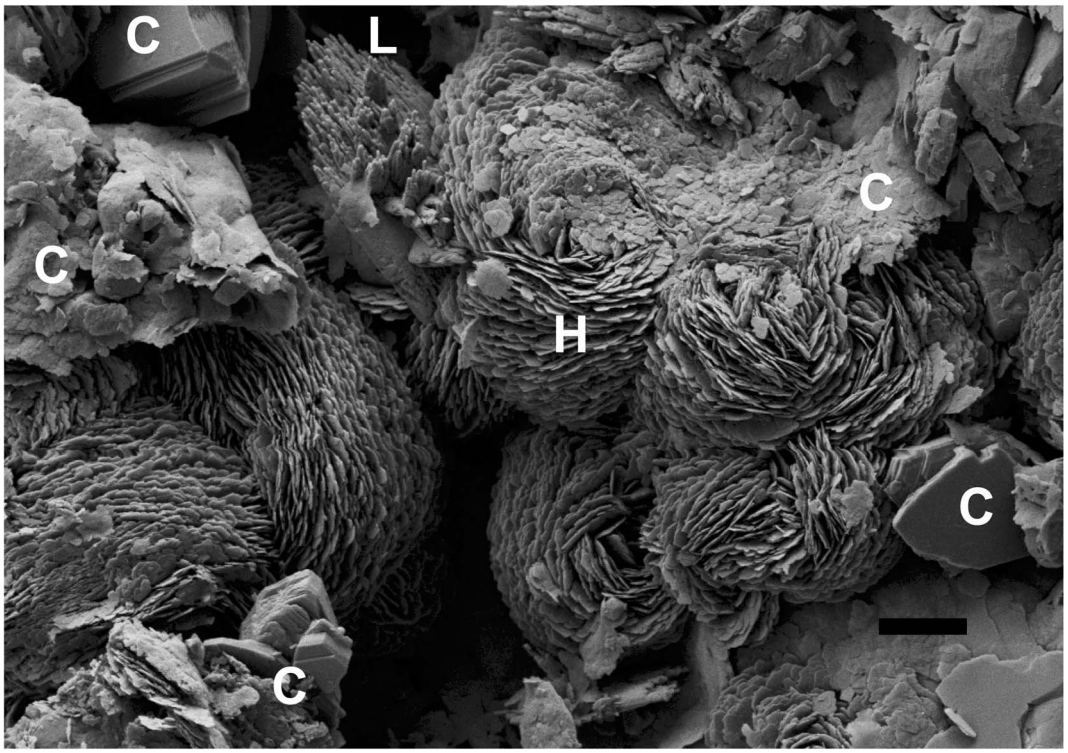

Fig. 3 SEM images of sample 470 (scale bar = 1 μm). Examples of typical mineral morphologies in NATH samples, showing FeOOH laths (indicated by the letter "L", upper middle left), hematite rosettes made from nanoscale platelets (H, dominating across the middle height of the image), and clays of various types distributed around the image (C).

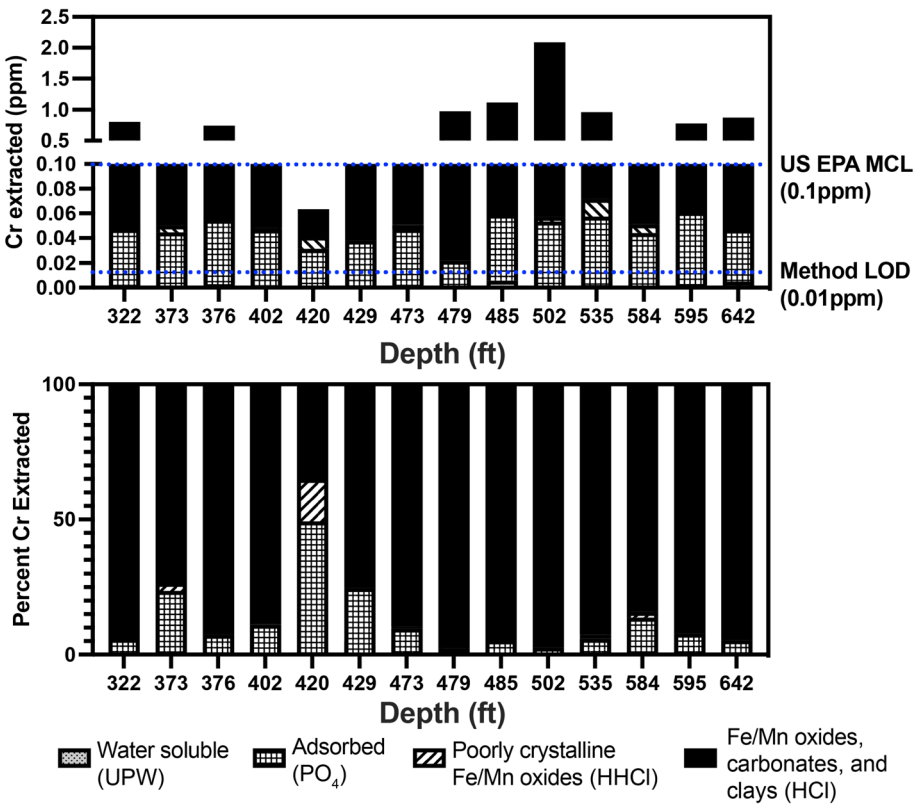

Fig. 4 Results of the sequential chromium extractions. Detection limit for total Cr was 10 μg L^{-1}, such that water soluble (UPW) and Fe/Mn-oxides (HHCl) extracts were too low to determine accurately in many samples.

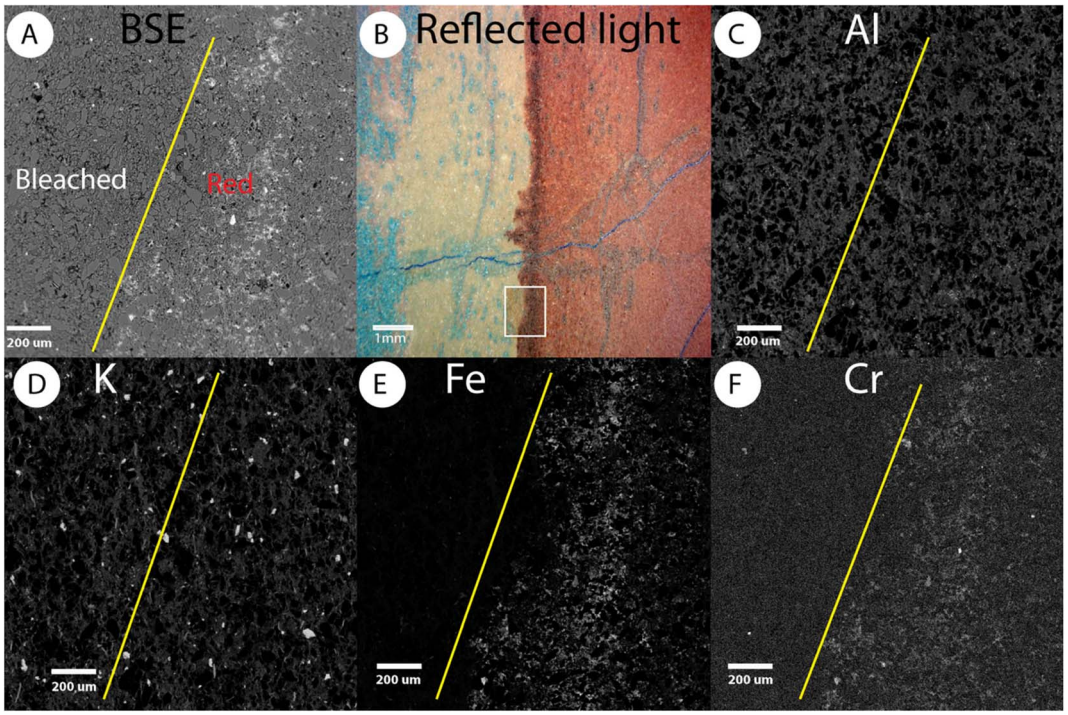

Fig. 5 X-ray intensity maps for thin section 323. (A) Backscattered electron image of the map area. (B) Optical thin section image with the EPMA map area outlined by the yellow box; blue staining was added during thin section preparation to highlight porosity. (C)–(F) Are X-ray intensity maps for aluminum, potassium, iron, and chromium, respectively. Areas that appear brighter contain a higher concentration of the respective element. For Al, Si, and K, there is no difference in concentration between the red and bleached areas. The Fe and Cr maps show that these elements are more concentrated in the red area.

sections (*e.g.*, 323 ft, Fig. 5; 502 ft, not shown; 591 ft Fig. S3†) by EPMA spot analyses, traverses, and X-ray intensity mapping demonstrated a correlation between Cr and Fe, but do not show a correlation between Cr and Al. SEM and XRD analyses of Fe-rich areas in sandstone samples indicated hematite dominated the crystalline Fe-oxide pool in most cases, although nanoscale goethite laths were also clearly present in some cases (*e.g.*, Fig. 3). Thus, hematite is the primary host for Cr (as Cr(III)) in the sandstone samples and likely the dolomitic conglomerate as well.

Dissolution of Mn-bearing dolomite as a source on Mn-oxides in sediment

Mn oxides have been reported as a mechanism for Cr(III) oxidation from studies performed in soils and Mn-oxides have been reported in COA cores in previous studies.[44,49] Moreover, aqueous Mn-concentrations in the COA are generally below detection limit, which is expected given the observed levels of dissolved oxygen and other redox-sensitive elements in the COA.[46] Therefore, most of the Mn in the COA must exist in the sediments. There are two main hosts for Mn in COA sediments, (1) Mn-bearing dolomite and (2) Mn-oxide minerals. Dolomite, which occurs as isolated nodules or as cements in sandstones, frequently contains up to ~1 wt% Mn (Fig. 6B).[49] The concentration of Mn oxides was below the detection limit for powder X-ray diffraction within the NATH core samples studied here (full XRD results presented in Table S2†) and individual Mn oxide crystals were not detected by SEM imaging, only enrichments in X-ray maps indicative of Mn oxides. However, we used a common chemical test from the soils literature, the net chromium oxidation potential, to estimate the concentration of Mn oxides (see Materials and Methods). The tests showed the extent of added Cr(III)(aq) reaction with sediments, related to the abundance of Mn oxides, is inversely proportional to the bulk Cr (Fig. 7A). This relationship indicates that areas within the NATH core with more manganese oxides contain lower bulk Cr concentrations remaining in the sediments, as would be expected if oxidation by Mn-oxides liberated Cr from iron oxides leading to aqueous dispersal of Cr(VI).

The results of the selective Mn-oxide dissolution experiments are more difficult to interpret, partly due to interference from Mn in carbonates. When results from all samples are plotted together, no trends exist between Mn and bulk Cr in the rock. However, when the samples are divided by lithology into sandstone and mudstone, a pattern emerges. The sandstones and mudstones each display a general inverse logarithmic relationship between Mn and Cr (Fig. 7B), with mudstones containing a greater proportion by mass of (hydr)oxides and clays (thus Cr) compared with sandstones. As observed in the Net Cr oxidation potential measurements, a negative correlation between Mn and Cr within the solid aquifer material would be expected if oxidation of Cr by Mn-oxides were occurring.

We identified etched dolomite surrounded by Mn accumulations *via* electron beam analyses similar to those noted by

 This journal is © The Royal Society of Chemistry 2022

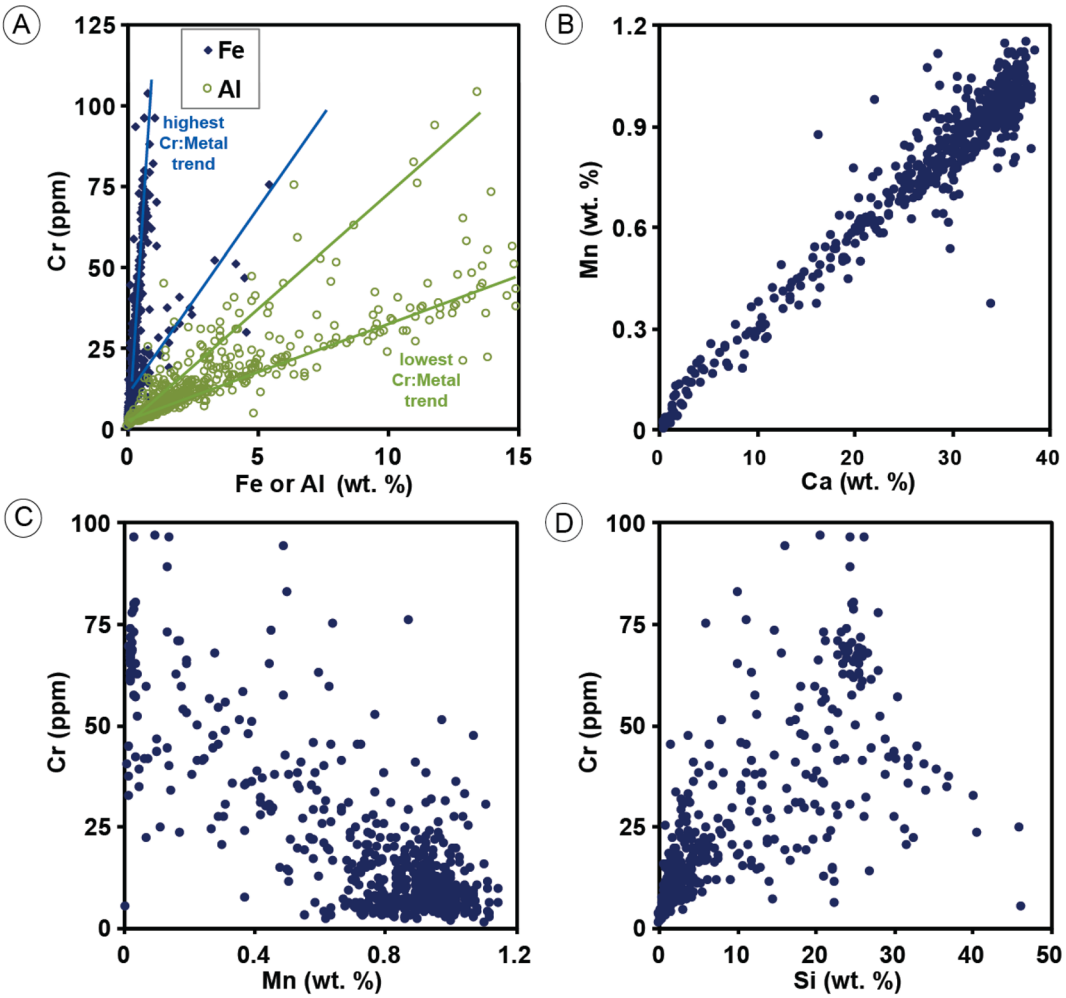

Fig. 6 LA-ICP-MS elemental correlations from dolomitic conglomerate thin section 473. Each data point represents an analysis from a single ablated spot. (A) The amount of Cr in the ablated rock areas as a function of either weight percent Fe (solid diamonds) or Al (open circles) demonstrating that Cr content rises much more rapidly with Fe than Al. (B) Mn occurrence scales with Ca content due to Mn(II) incorporation in the dolomite. (C) Ablated regions high in Mn tend to be low in Cr, due to the presence of Mn(II) but not Cr in dolomite. (D) Cr shows no apparent trend with Si.

Breit *et al.* with SEM/X-ray analyses of COA core samples collected for a previous study[50] (Fig. 8). The spatial distribution of Mn in energy-dispersive X-ray maps on the polished rock section correlates with (1) backscattered electron image brightness and Fe, indicative of Mn and Fe-oxides in the pore spaces, and (2) the distribution of Ca and Mg, indicative of the Mn-bearing dolomite. Further XRD and SEM/X-ray spectroscopy results confirm the presence of Mn-dolomite, with Mn-oxides generally too low in abundance to detect (*e.g.*, Fig. S4†).

In summary, we have direct evidence of Mn oxide formation associated with Mn-bearing dolomite dissolution (Fig. 8) and indirect evidence for the presence of Mn oxides through selective extraction and Cr(III) oxidation. Hydrogeochemical models by the U.S. Geological Survey[44] point to Mn-bearing dolomite dissolution, and we know that while Ca and Mg are abundant at near-equal proportions as expected from equilibrium with dolomite and Mn concentrations were below detection limits, pointing to a missing reservoir of Mn in the aquifer.

Statistical evaluation of COA aquifer hydrochemistry

Single-variable relationships between major ions, biogeochemical parameters (pH, DO, *etc.*) did not reveal any clear relationships with pH, thus multivariate methods were applied. First, hierarchical clustering was performed, separating groundwater analyses into 5 independent clusters. Then, PCA analyses were performed to explore relationships between groundwater parameters and the independent cluster membership (Fig. 9). Descriptive statistics for each cluster are presented in Table 1, and data organized by cluster membership are presented in the PCA diagram (Fig. 9), a pH/Cr plot (Fig. 10) and Piper diagram (Fig. 11). Members of clusters 1, 2, and 3 are lower in Cr, while clusters 4 and 5 contain all groundwaters with Cr > 50 ppb (Fig. 10, Table 1). Members of clusters 1–3 have median and interquartile ranges of Cr less than 15 ppb, while median Cr values are 20 and 60 for clusters 4 and 5, reaching maximum values of 120 and 130 ppb, respectively. The lower median Cr value of cluster 4 at 20 ppb is

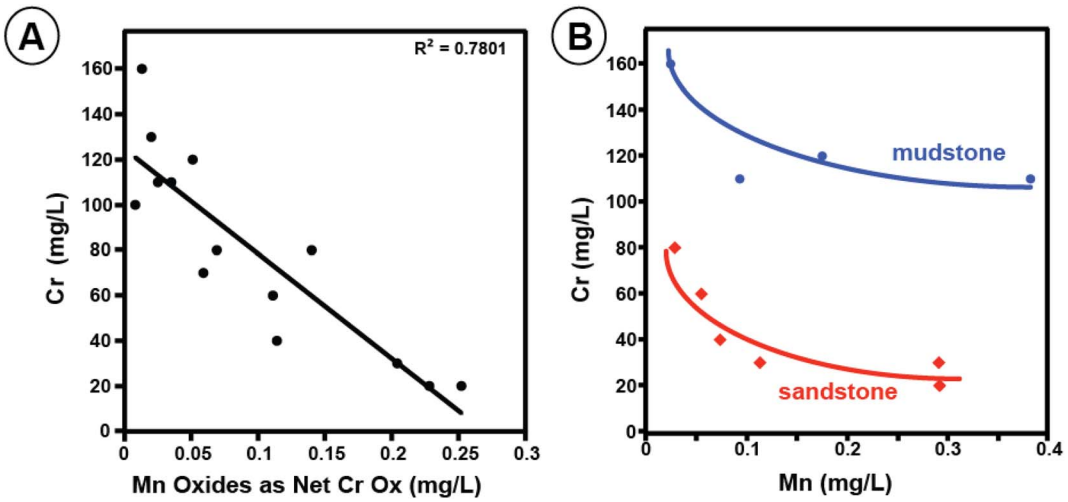

Fig. 7 Results of the net chromium oxidation potential (A) and the selective Mn dissolution treatments (B). In (B), the upper trend (blue, circles) represents extracted Mn and Cr from mudstone core samples, while the lower trend (red, diamonds) analyses were extracted from sandstones. Trend lines in (B) do not imply the presented trend is statistically significant. Values in both correspond to the aqueous concentrations in treatment supernatants.

interesting in the light of the pH *vs.* Cr plot (Fig. 10), which demonstrates that despite many of the elevated Cr groundwaters belonging to cluster 4, many of the high pH/cluster 5 samples have very low Cr, and pH is not a good predictor of Cr content in the groundwater. This is in contrast to the behavior of arsenic, where groundwater pH is a useful predictor of elevated As concentrations due to desorption from iron oxide minerals.[44]

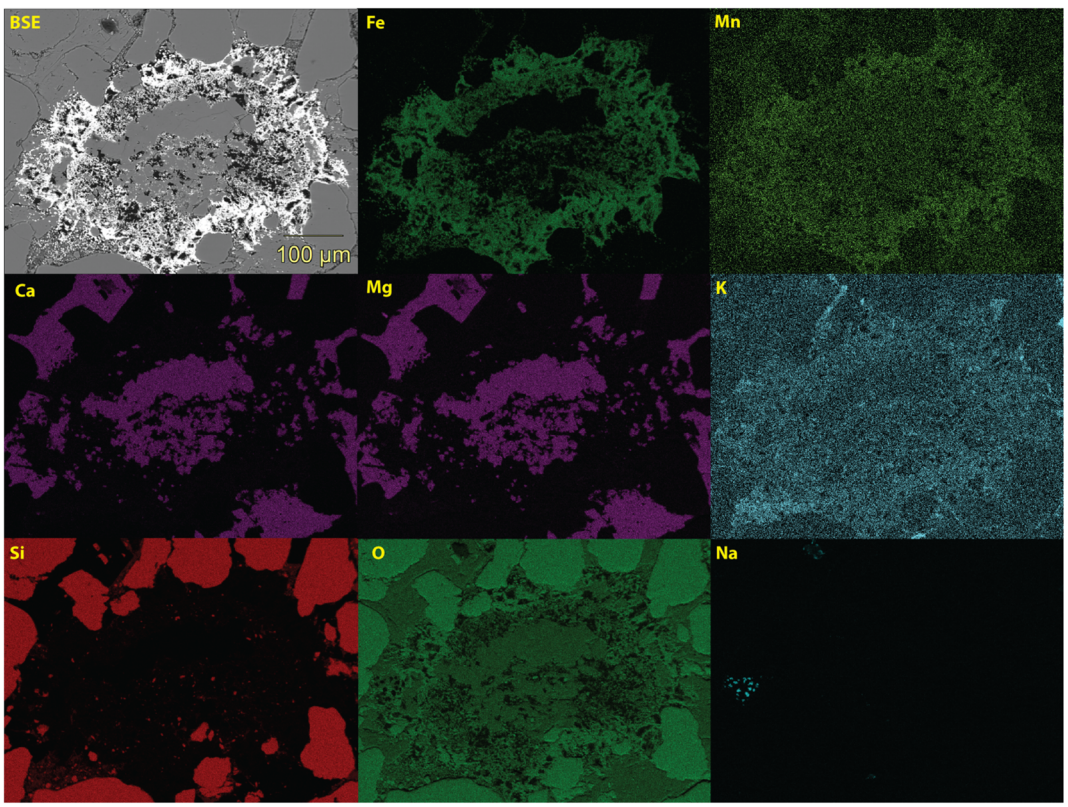

Fig. 8 Backscattered electron image and energy dispersive X-ray elemental maps from a Norman Arsenic Test Hole Core sample at 350 feet depth. Note the elevated Mn in regions of elevated Fe within the weathered texture and porosity around the dolomite grain, while also being present in the dolomite as well.

 This journal is © The Royal Society of Chemistry 2022

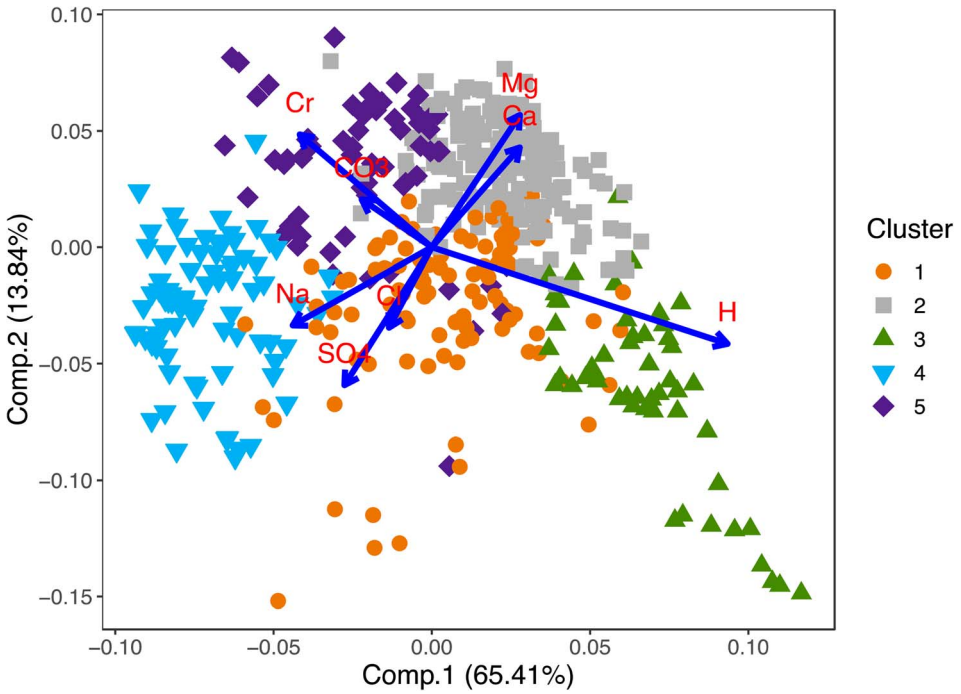

Fig. 9 PCA analysis of groundwater data, symbol shape/colors according to cluster membership.

The three low-Cr clusters have unique geochemical characteristics, with overlapping values in many parameters (Fig. 11, Table 1). Cluster 1 has much higher median Na and Cl concentrations compared with clusters 2 and 3. Cluster 2 is intermediate in most parameters, while cluster 3 members have a median pH more than one pH unit lower than clusters 1 or 2 (Table 1). Cluster 3 also has a much lower median Ca, Mg, and carbonate concentrations than any other cluster.

The two clusters with higher median Cr values (4 and 5) are also separated by differences in other geochemical parameters. Both clusters have much lower median Ca and Mg concentrations than clusters 1–3. However, median Ca and Mg values for cluster 4 are ~one order of magnitude lower than cluster 5, consistent with the decreasing solubility of carbonate minerals with increasing pH. Cluster 4 also has the highest median Na concentrations of any cluster, despite having relatively low Cl

Table 1 Bootstrapped median values of parameters from each cluster using the 'boot()' package in R with 5000 iterations. Although methods that specifically account for censored data are generally preferred,[57] the individual values below reporting limits were unrecoverable due to changing reporting limits through the dataset. Therefore, the regular bootstrap function was used; values below reporting limits were replaced with half of the reporting limit value before bootstrapping to mitigate the normal right or left skewness which comes with replacing a bdl value with 0 or the reporting limit, respectively. Full descriptive statistical values are provided in the ESI. Calculated saturation index values from thermodynamic modeling are reported for relevant mineral phases

Cluster	Unit	1	2	3	4	5
pH		7.4	7.5	6.3	8.8	7.97
Cr	μg kg^{-1}	<15	<10	<10	20	60
Ca	mmol kg^{-1}	1.55	1.17	0.7	0.06	0.35
Mg	mmol kg^{-1}	1.19	1.07	0.49	0.04	0.45
Na	mmol kg^{-1}	4.79	0.78	0.84	7.57	3.79
K	mmol kg^{-1}	<0.05	<0.05	<0.03	<0.05	<0.05
CO_3	mmol L^{-1}	3.04	2.31	1.26	3.13	2.49
Cl	mmol kg^{-1}	2.23	0.34	0.49	0.37	<0.28
SO_4	mmol kg^{-1}	0.43	0.1	0.2	0.37	0.11
SiO_2	mmol kg^{-1}	0.24	0.12	0.27	0.17	0.22
Dolomite (disord.) SI		−0.25	−0.25	−3.69	−0.3	−0.08
Calcite SI		0.26	0.25	−1.5	0.24	0.28
Gypsum SI		−2.38	−2.99	−2.76	−3.69	−3.27
Ca/Mg mol ratio		1.1	1.1	1.3	1.2	0.7
Na/Cl mol ratio	—	2.2	2.3	1.7	20.5	>13.5

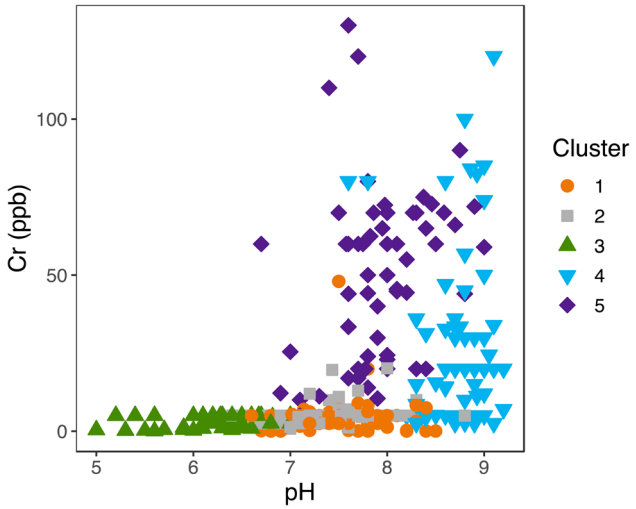

Fig. 10 Total dissolved Cr *vs.* pH in COA groundwater. Measurements include those with depth-specific isolation of formation water only, corresponding to groundwater primarily from a known depth. Many wells in the COA are perforated at multiple intervals; thus, the wellhead chemistry reflects a mixture of different biogeochemical processes occurring spatially and temporally separated in the aquifer.

values. Cluster 5, as demonstrated by the PCA plot (Fig. 9), is most influenced by the elevated Cr in the cluster analysis. Cluster 5 is also characterized by Na >> Ca and Mg, although uniquely has the lowest median Ca/Mg ratio of 0.7, compared to 1.1–1.3 observed in the other clusters, indicating a depletion of Ca relative to Mg. The Piper diagram (Fig. 11) shows clear separations between the two clusters with higher Cr, clusters 4 and 5. For example in the cation ternary (Fig. 11, lower left triangle), the uniquely high cluster 4 Mg/Ca ratio trend towards the Na corner, while cluster 5 plots dominantly in the Na corner. Also, in the water type diamond (Fig. 11 upper, middle), cluster 5 plots along a trend between a Na-bicarbonate and Na-sulfate/chloride water types, while cluster 4 follows a separate trend between the Mg-bicarbonate and Na-bicarbonate water types.

Spatial analysis of COA aquifer hydrochemistry

The spatial distribution of groundwaters included in each cluster varies with depth, latitude, and longitude (Fig. 12). Cluster 1 members spans depths from shallow to deep, with a wide interquartile range, while other clusters mostly contain members from a more constrained depth range: cluster 2 throughout the shallow aquifer range, cluster 3 from a very narrow range of very shallow wells, and both cluster 4 and 5

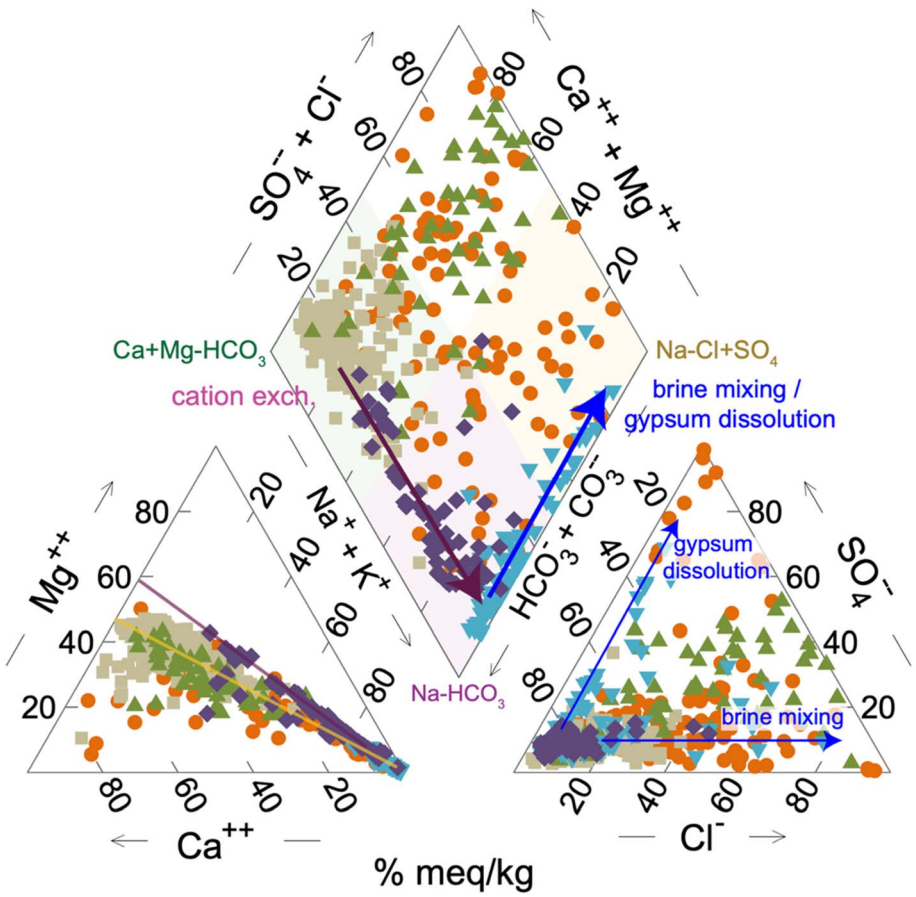

Fig. 11 Piper diagram of groundwater samples with symbol/color by cluster membership as in previous figures. Purple arrows show trends consistent with cation exchange; the yellow line is more characterized by mixing with connate waters; the blue arrow represents bring mixing and gypsum dissolution.

 This journal is © The Royal Society of Chemistry 2022

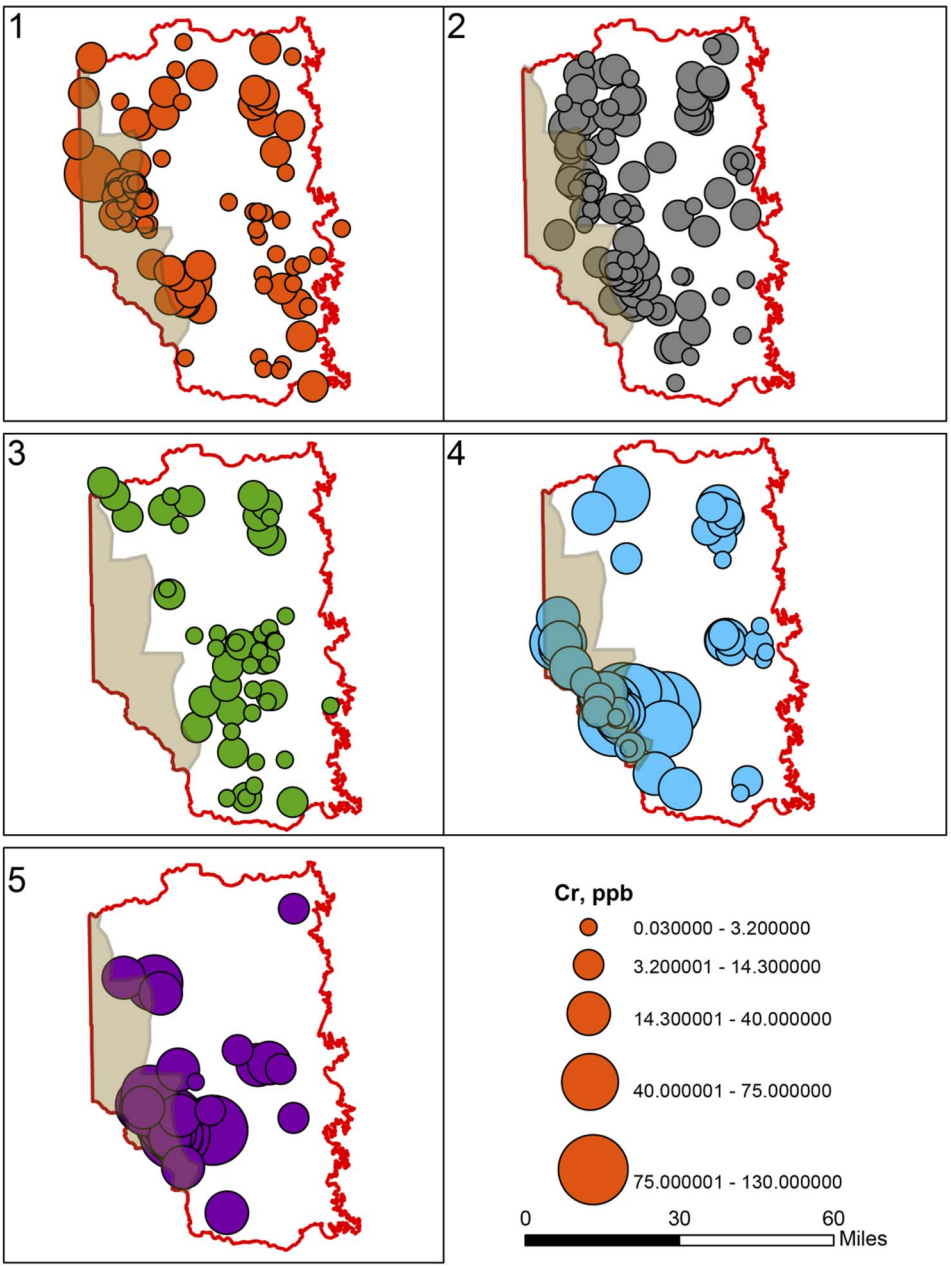

Fig. 12 Spatial map-view distribution of membership in each cluster, with the symbol size as a function of Cr concentration. Symbol size bins were calculated using the 'natural break' function in R to distribute the points evenly. The Hennessey formation confining layer surface exposure outline is indicated by the shaded area on the western side of the maps.

from exclusively deep aquifer samples (Fig. 13, left). As groundwater age correlates with depth in the COA,[46] we infer that cluster 3 includes very young waters. Cluster 2 mostly younger waters, cluster 1 a range of young to old groundwaters, and clusters 4/5 exclusively older groundwaters with greater water–rock contact time. Furthermore, groundwaters with elevated Cr are almost exclusively found in groundwaters from cluster 4 or 5 at depths >400 ft.

Surface locations of cluster members and corresponding Cr contents follow unique patterns for each cluster in map view, generally following north-south trends that parallel regional stratigraphic dip (Fig. 14). Groundwater with elevated chromium is concentrated on the southwestern, confined part of the aquifer; other members of cluster 4 and 5 also are found in north–south trending bands towards the west and eastern margins, with cluster 5 members closest to the western edge and farthest underneath the overlying Hennessey formation. Cluster 1 overlaps somewhat with the general trend of cluster 5, but with a greater population in the northwest rather than southwest. Wells with cluster 2 members are distributed throughout the aquifer, except less on the western/southwestern margins, and wells with groundwaters in the shallow cluster 3 fall predominantly along a central north–south band.

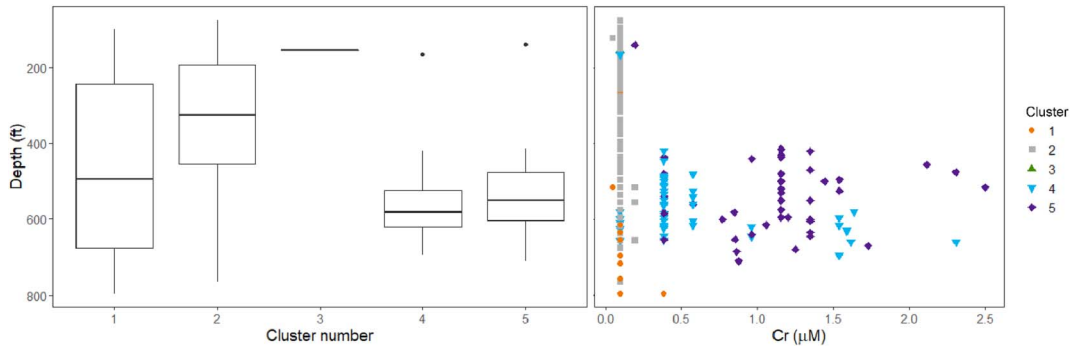

Fig. 13 (Left) Boxplot diagram illustrating sample depth by cluster membership and (right) Cr concentration as a function of sample depth, color/symbol coded according to cluster membership.

2D mapping and depth-dependent sampling both help delineate members of cluster 4 that are very low in Cr. A cross-section through the southwestern region of the aquifer that contains many of the greatest chromium concentrations demonstrates that there is a strong east-west dependence (Fig. 14). Members of clusters 4 and 5 with lower chromium are found in the farthest west, in the most strongly confined area, where the influence of the overlying gypsum-bearing Hennessey formation may influence the aquifer geochemistry, as suggested by the increase in sulfate shown on the Piper plot (Fig. 11).

Clustering provides evidence for the importance of cation exchange and dolomite dissolution linked to Cr occurrence

Previous studies of the COA concluded that cation exchange promoted dolomite dissolution.[44,46] The nearly 1 : 1 calcium–magnesium molar ratio in groundwater samples provided evidence for dolomite dissolution as a dominant process controlling aquifer biogeochemistry.[46] Furthermore, clay minerals within core samples were shown to have dominantly Na in the exchangeable fraction, dominated by mixed-layer illite–smectite.[48] In the case of arsenic, a general conceptual model was proposed that explained occurrences: increased carbonate dissolution leading to increasing pH, with subsequent pH-dependent desorption of arsenic from iron oxide minerals.[58] Groundwaters with elevated chromium escape such straight-forward linkages to a single parameter such as pH (*e.g.*, Fig. 10). In this study we suggest that the dissolution of dolomite due to cation exchange are also linked to chromium occurrences, but through intermediate 'cryptic' manganese cycling. Mn switches between various solid-phase pools with

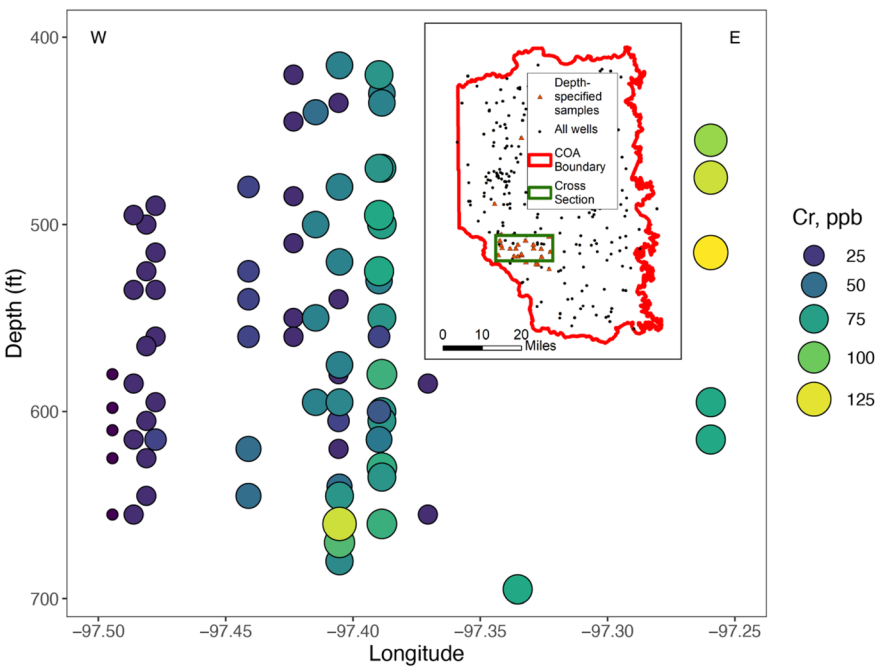

Fig. 14 Cross-sectional view of cluster 4 and cluster 5 data showing chromium concentration based on the color/size of bubble. The depth-longitude location of the sampled groundwater samples are indicated in reference to the area shown on the inset map. Groundwaters farthest to the west and deep underneath the Hennessey confining unit have Cr values less than those ~−97.40 longitude.

 This journal is © The Royal Society of Chemistry 2022

only transient presence in the aqueous/soluble pool, such that it is not measured in typical groundwater sampling.

Although a suite of groundwater biogeochemical parameters was used in the hierarchical clustering analysis, pairwise considerations are also useful for interpreting processes and trends with data available for this study (Fig. 15). Pairwise relationships (Fig. 15) indicate the importance of cation exchange, demonstrate brines are not responsible for elevated chromium, and suggest the need for long rock–water contact times.

We propose a conceptual model where soluble groundwater Cr increases correlate with cation-exchange driven dolomite dissolution, occurring along deep flowpaths primarily under or near the western, confined portion of the aquifer (Fig. 16, purple box). Shallow waters are in equilibrium with dolomite and experience little ongoing dissolution (Fig. 16, red box), while deeper eastern waters show evidence for mixing with the underlying brine and diluting the Cr concentration (Fig. 16, blue box). Data point color in Fig. 15 corresponds to cluster membership as in previous figures, while the arrows highlighting trends correspond to the color of the boxes highlighting physical aquifer locations in Fig. 16.

Clusters exhibit different trends for Na *vs.* Mg or Ca activity (Fig. 15A and B) and Ca/Mg activities (Fig. 15C). Clusters 2 and 3 have steep slopes on Na–Ca and Na–Mg plots (Fig. 15A and B), indicating dolomite dissolution adds both Ca and Mg to these groundwaters, but the limited activity of Na is consistent with the generally shallow depths of the wells and/or sampled intervals and accordingly young water ages. Major sources of Na observed in these groundwater samples are slow dissolution of Na-silicates such as plagioclase feldspar (as seen in our study and others), cation exchange with Na-bearing clays, and mixing with brines below the aquifer. Clusters 1 and 5 show decreasing Ca and Mg with increasing Na (Fig. 15A and B). This is consistent with both cation exchange and decrease in carbonate mineral solubility at higher pH values; higher pH in turn

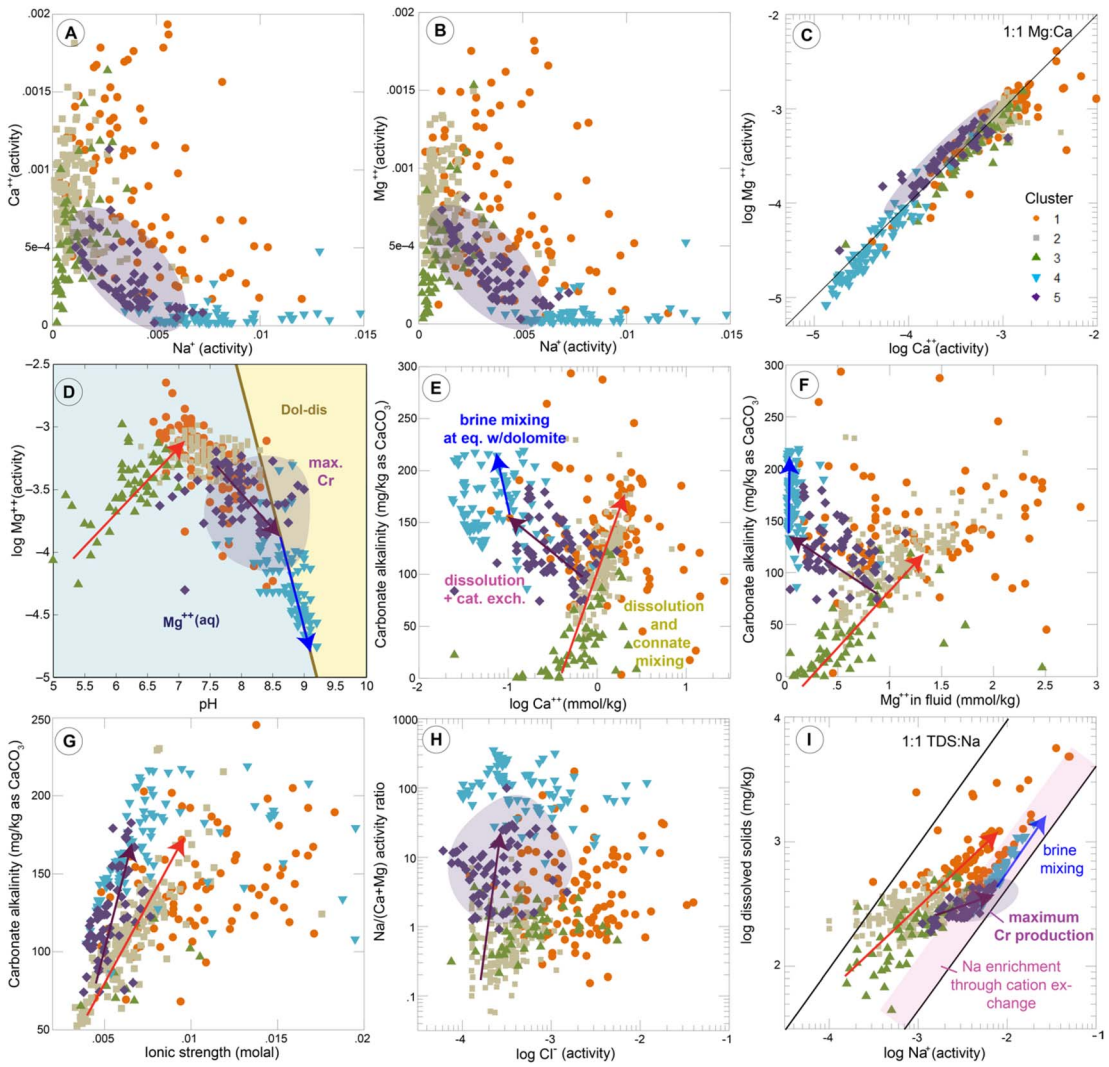

Fig. 15 (A–I) Groundwater chemical relationships, symbol according to cluster membership. Note some axes are linear while others are log. In (F), phase boundaries were calculated in Geochemist's Workbench. Samples from cluster 5 (purple) had the highest average Cr concentrations. Orange arrows represent trends consistent with carbonate dissolution in undersaturated conditions and mixing with connate waters.

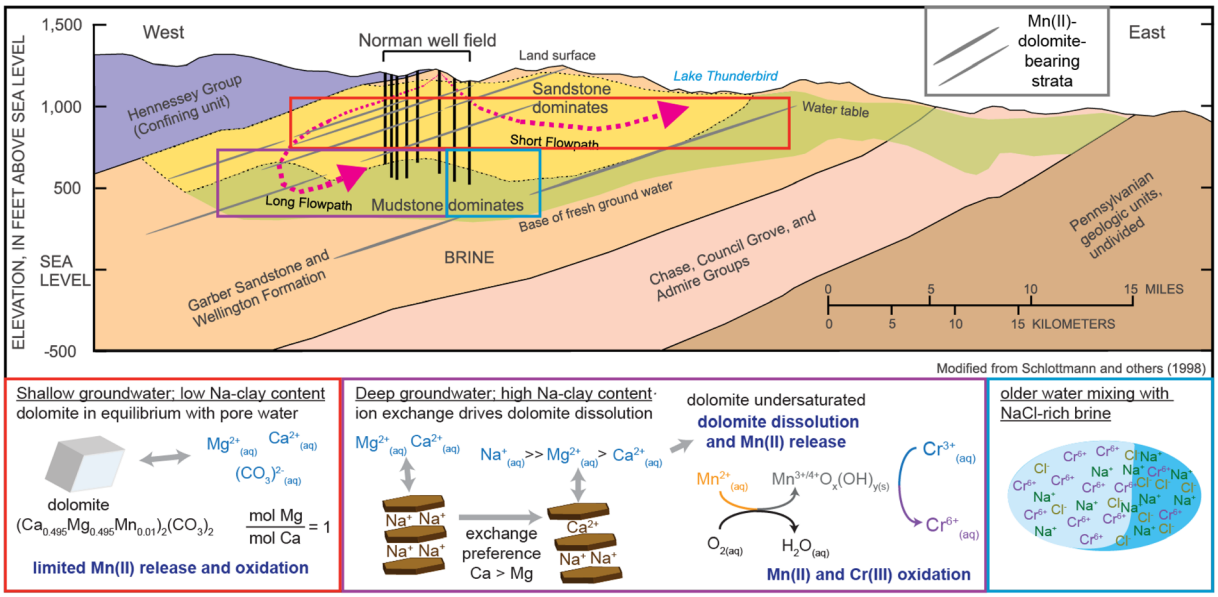

Fig. 16 Sequential steps of the hypothesized conceptual model for Cr(III) oxidation by Mn oxides in the COA. Processes occurring in boxed areas in the cross-section are described in the corresponding color boxes below, which also match colors from previous figures describing COA groundwater chemistry.

correlates with elevated Na. Cluster 4 members follow a trend of maintaining low divalent cation activities while Na is high and increasing.

Cluster 5, with highest median Cr, shows evidence of active cation exchange. Ca and Mg activities decrease with increasing Na, consistent with divalent ions Ca^{2+} or Mg^{2+} from solution replacing Na^+ bound to exchangeable sites in clays, by two Na^+ added to groundwater for each Ca^{2+} or Mg^{2+} removed. During the exchange process, Ca is slightly preferred over Mg by the clay, leading to a slight excess of Mg in solution.[59,60] Cluster 5 shows this behavior, with the lowest bootstrapped median Ca : Mg molar ratio (0.7), indicating an excess of Mg in solution, while all other clusters have slight Ca excesses (1.1–1.3) (Table 1). The unique cluster 5 trend in Na, Ca, Mg is also visible in the Piper plot (Fig. 11).

Cluster 4 groundwater samples show evidence for having passed through a Cr-generation stage, but in some cases the Cr may have been subsequently diluted by mixing with a Cr-poor brine. Cluster 4 members likely contain the oldest and most chemically evolved groundwaters, as seen by the high pH and Na but low Mg and Ca values (Table 1, Fig. 15A–C). Some cluster 4 groundwater Mg : Ca ratios greater than 1 may be associated with gypsum dissolution on the western, confined part of the aquifer underneath the Hennessey Formation (Fig. 11 and 15C). The very low cluster 4 Ca and Mg concentrations likely also relate to the decreasing solubility of dolomite at higher pH values (Fig. 15D). Many cluster 4 values follow the calculated phase boundary for disordered dolomite calculated for elevated pH conditions, indicating these groundwaters are in equilibrium with disordered dolomite (Fig. 15D).

Given the hypothesis that dolomite dissolution controls Mn release rate and thus Cr(III) oxidation, dolomite solubility trends are important. The solubility of dolomite is affected by pH as well as other components of the solution, represented by a range in Fig. 15D. The maximum groundwater Mg^{2+} activities are likely related to dolomite solubility for all clusters (Fig. 15D). The bootstrapped median disordered dolomite (dol-dis) SI values are closest to zero/equilibrium for cluster 4 (−0.08, Table 1), but near equilibrium for clusters 1 (−0.25), 2 (−0.25), and 5 (−0.30). Only cluster 3, the shallow groundwaters (Fig. 13) with acidic pH values (Fig. 10) are significantly undersaturated with respect to dolomite dissolution (median dol-dis SI = (−3.69)).

Ca and Mg activities *versus* alkalinity show dolomite dissolution is an important process for all clusters, but clusters 4 and 5 follow distinct trends particularly due to cation exchange (Fig. 15E and F). Ca and Mg increase with increasing alkalinity for most members of clusters 1–3. On the other hand, cluster 5 Ca and Mg activities decrease with increasing alkalinity. Ca and Mg values are very low for cluster 4, showing relatively less change in Ca/Mg over a large change in alkalinity values (Fig. 15E and F). There are some overlaps with cluster 1 and 3 members with cluster 5 on Fig. 15E and F; clusters separate more clearly when plotting alkalinity related to ionic strength (Fig. 15G). This relationship shows that the elevated-Cr groundwaters (cluster 4 and some of cluster 5) show higher alkalinity at lower ionic strength than clusters 1–2, suggesting a greater proportion of the mineral–water interactions are attributed to dolomite dissolution.

Thus, key components of elevated Cr include a dominance of dolomite dissolution in mineral–water interactions paired with a signature of cation exchange, as described above and illustrated by Fig. 15H. Groundwaters with the most elevated Cr have high Na/(Ca + Mg) activity ratios at low Cl (Fig. 15H). Cl concentrations are a proxy for mixing with connate groundwater related to ancient seawater evaporation in the present-day COA

 This journal is © The Royal Society of Chemistry 2022

region.[46] Cluster 4 members then represent dilution with brine rich in Na, Cl, and in some cases SO_4 (Fig. 11).

Cation exchange increases Na but not total salinity and chloride; whereas brine mixing would be expected to increase Na, TDS, and Cl simultaneously. Cluster 5 waters (those most frequently having high Cr) reach a high Na activity at low TDS, consistent with ion exchange (Fig. 15I). Many cluster 4 samples then follow the 1 : 1 TDS : Na trend, demonstrating brine mixing influences cluster 4 groundwaters. Interestingly, some cluster 1 groundwaters plot with cluster 4 on the Na-enriched trend in Fig. 15I, indicating possible mixing with brines. However, they plot separately on Fig. 15G and H; cluster 1 groundwaters have a greater Cl/brine signature than cluster 4 for the same alkalinity indicating that cluster 1 groundwaters have not been in contact with as many carbonate minerals. Cl and SO_4 having the greatest positive influence on cluster 1 in the PCA plot (Fig. 9), rather than carbonate. Thus cluster 1 groundwaters have both low Cr and have experienced the least amount of carbonate dissolution.

Synthesis and key findings

Our investigations of a redbed aquifer containing elevated groundwater chromium content, a large fraction of which is Cr(VI), led to the following key findings:

(1) The redbed aquifer sediment contains a majority of Cr as Cr(III) substituted in Fe(III)-oxides. To our knowledge, this is the first confirmation of Cr(III) for Fe(III) substitution in iron oxide minerals dominating the Cr pool in a deep redbed clastic aquifer, requiring an oxidation process to explain aqueous Cr(VI) occurrences.

(2) Chromium cycling is linked to dissolution of Mn-bearing dolomite. It is widely accepted that Mn-oxides are the primary naturally occurring compounds that are known to initiate the direct oxidation of trivalent chromium to hexavalent chromium.[9,24,26,61–63] Furthermore, the capacity for Mn(III/IV) oxides to participate in redox reactions is proportional to their age: fresh Mn oxides tend to have a greater proportion of Mn(III), a more highly disordered crystal structure, and greater chemical reactivity.[27,64] COA rocks contain dolomite-bearing zones with significant amounts of manganese (~1 wt% as Mn(II)[49]), as confirmed in our LA-ICP-MS (Fig. 6D) and energy-dispersive X-ray analyses (Fig. 8). Dolomite dissolution releases Ca(II), Mg(II), Fe(II), Mn(II), and increases pH values. However, dissolved Mn or Fe is not observed in groundwater samples above the reporting limit, indicating that once Mn(II) enters the alkaline oxic COA groundwater, it is oxidized to insoluble Mn(III/IV) oxides. While Mn oxides are forming, the Fe(II) also released from dolomite should initiate re-crystallization of pre-existing iron oxides,[65–68] releasing trace amounts of Cr(III) incorporated into their crystal structures, then re-crystallizing as goethite. The presence of nanoscale goethite laths collected from groundwater[69] provides evidence for such active iron cycling within the aquifer. Once in the groundwater, some of the Cr(III) likely precipitates as $(Fe,Cr)(OH)_3$ solid solutions[70–72] or sorbs onto any negatively charged aquifer sediment grains, such as Mn-oxides.[37] A small fraction also remains as soluble $Cr(III)_{(aq)}$ which could be adsorbed onto the surfaces of Mn-oxides, where it may oxidize to Cr(VI).[12] Mn(II) released from dolomite dissolution may also participate in direct oxidation of mineral-hosted Cr(III).[34] The produced Cr(VI) would be soluble and susceptible to desorption, especially in groundwaters with pH > 8.5. Our study uniquely suggests that the dissolution of Mn-bearing carbonate serves as the source of Mn in a drinking water aquifer, as the occurrence of Cr(VI) is linked to the intensity of Mn-dolomite dissolution *via* cation exchange.

(3) Groundwater production of Cr is linked to cation exchange. A majority of aquifer groundwaters are near saturation with respect to dolomite. The data suggest that cation exchange drives dolomite dissolution in deep, relatively dilute (low ionic-strength) groundwaters. Perhaps these groundwater conditions are also ideal for Mn-oxidizing bacteria, although no data on microbial activity is available. Occurrences of elevated Cr occur below ~450 ft (~137 m) (Fig. 12). This depth corresponds to regional changes in flow behavior, previously ascribed to a greater dominance of clay-rich mudstone and exchangeable clays.[44]

Implications

As the chemistry of many aquifer systems throughout the world involves carbonate mineral precipitation and dissolution, the links between Mn-bearing dolomite, cation exchange, and Cr occurrence demonstrated in the COA may provide insights for the cycling of chromium in other carbonate aquifer systems as well. This study demonstrates that the presence of exchangeable clays may lead to hot-spots of groundwater chromium when paired with Mn-bearing carbonate minerals. Furthermore, these linkages may be important for groundwater management processes such as Managed Aquifer Recharge (MAR).[73] Injection of waters with different salinity or pH may cause dissolution of Mn-bearing carbonate minerals that then may interact with trace metals. The concentration of Mn in Mn-carbonates required to produce Mn oxides that will mobilize trace metals in aquifers is unknown. However, the incorporation of Mn in carbonates is extremely common[74] including concentrations of ~1% Mn[75] as in the COA, suggesting the need to examine Mn-carbonate – exchangeable clay – trace metal connections.

Author contributions

The manuscript was written through contributions of all authors. All authors have given approval to the final version of the manuscript.

Conflicts of interest

There are no conflicts to declare.

Acknowledgements

This research was supported by the University of Oklahoma Vice President for Research and the Schultz Chair. George Morgan,

Lindsey Hunt, and Preston Larson assisted with EPMA and SEM analyses. Molly Sexton, Sarah Van Deventer, Shelbie Bartlett, Brian Gallagher, Virginia Priegnitz, and Brett Weeks provided assistance at various stages of research, including XRD, BET, and SEM analysis for some of the core samples. Shana Mashburn (U.S. Geological Survey), Ken Komiske, Geri Wellborn, and Chris Mattingly (City of Norman) provided logistical support and/or data. This work is not a product of the United States Government or the United States Environmental Protection Agency. Co-authors Maples did not do this work in any governmental capacity. The views expressed are his own and do not necessarily represent those of the United States or the US EPA.

References

1 J. Guertin, J. A. Jacobs and C. P. Avakian, *Chromium (VI) handbook*, CRC Press, 2005.
2 E. L. Hawley, R. A. Deeb, M. C. Kavanaugh and J. A. Jacobs, in *Chromium (VI) Handbook*, ed. J. Guertin, J. A. Jacobs and C. P. Avakian, CRC Press, 2005, pp. 276–309.
3 J. W. Patterson, E. Gasca and Y. Wang, Optimization for Reduction/Precipitation Treatment of Hexavalent Chromium, *Water Sci. Technol.*, 1994, **29**, 275–284.
4 Q. Wang, N. Cissoko, M. Zhou and X. H. Xu, Effects and mechanism of humic acid on chromium(VI) removal by zero-valent iron (Fe^0) nanoparticles, *Phys. Chem. Earth*, 2011, **36**, 442–446.
5 Y. G. Chen, Y. He, W. M. Ye, C. H. Lin, X. F. Zhang and B. Ye, Removal of chromium(III) from aqueous solutions by adsorption on bentonite from Gaomiaozi, China, *Environ. Earth Sci.*, 2012, **67**, 1261–1268.
6 D. E. Crean, V. S. Coker, G. van der Laan and J. R. Lloyd, Engineering Biogenic Magnetite for Sustained Cr(VI) Remediation in Flow-through Systems, *Environ. Sci. Technol.*, 2012, **46**, 3352–3359.
7 H. R. Dong, Q. He, G. M. Zeng, L. Tang, C. Zhang, Y. K. Xie, Y. L. Zeng, F. Zhao and Y. A. Wu, Chromate removal by surface-modified nanoscale zero-valent iron: Effect of different surface coatings and water chemistry, *J. Colloid Interface Sci.*, 2016, **471**, 7–13.
8 S. Rajput, C. U. Pittman and D. Mohan, Magnetic magnetite (Fe_3O_4) nanoparticle synthesis and applications for lead (Pb^{2+}) and chromium (Cr^{6+}) removal from water, *J. Colloid Interface Sci.*, 2016, **468**, 334–346.
9 W. E. Motzer, in *Chromium (VI) Handbook*, ed. J. Guertin, J. A. Jacobs and C. P. Avakian, CRC Press, 2005, pp. 23–91.
10 U. S. E.P.A., *Chromium in Drinking Water*, **https://www.epa.gov/sdwa/chromium-drinking-water**.
11 Y. Xie, S. Holmgren, D. M. K. Andrews and M. S. Wolfe, Evaluating the Impact of the U. S. National Toxicology Program: A Case Study on Hexavalent Chromium, *Environ. Health Perspect.*, 2017, **125**, 181–188.
12 C. D. Palmer and R. W. Puls, *Natural attenuation of hexavalent chromium in groundwater and soils*, U.S. Environmental Protection Agency, Kerr Laboratory, 1994.
13 P. M. Jardine, T. L. Mehlhorn, W. B. Bailey, S. C. Brooks, S. Fendorf, R. W. Gentry, T. J. Phelps and J. E. Saiers, Geochemical Processes Governing the Fate and Transport of Chromium(III) and Chromium(VI) in Soils, *Vadose Zone J.*, 2011, **10**, 1058–1070.
14 J. M. Zachara, C. E. Cowan, R. L. Schmidt and C. C. Ainsworth, Chromate Adsorption by Kaolinite, *Clays Clay Miner.*, 1988, **36**, 317–326.
15 J. M. Zachara, D. C. Girvin, R. L. Schmidt and T. C. Resch, Chromate adsorption on amorphous iron oxyhydroxide in the presence of major groundwater ions, *Environ. Sci. Technol.*, 1987, **21**, 589–594.
16 H. Lai and L. S. Mcneill, Chromium redox chemistry in drinking water systems, *J. Environ. Eng.*, 2006, **132**, 842–851.
17 J. G. Kim and J. B. Dixon, Oxidation and fate of chromium in soils, *Soil Sci. Plant Nutr.*, 2002, **48**, 483–490.
18 G. R. C. Cooper, Oxidation and toxicity of chromium in ultramafic soils in Zimbabwe, *Appl. Geochem.*, 2002, **17**, 981–986.
19 C. M. Chon, J. G. Kim, G. H. Lee and T. H. Kim, Influence of extractable soil manganese on oxidation capacity of different soils in Korea, *Environ. Geol.*, 2008, **55**, 763–773.
20 E. Nakayama, T. Kuwamoto, S. Tsurubo and T. Fujinaga, Chemical speciation of chromium in sea water, *Anal. Chim. Acta*, 1981, **130**, 401–404.
21 A. Rajapaksha, M. Vithanage, Y. Ok and C. Oze, Cr(VI) Formation Related to Cr(III)-Muscovite and Birnessite Interactions in Ultramafic Environments, *Environ. Sci. Technol.*, 2013, **47**, 9722–9729.
22 D. S. Ross, H. C. Hales and A. Lanzirotti, Oxidation of Added Mn(II) in Soils Observed by XANES Spectroscopy and Cr(III) Oxidation, *Soil Sci. Soc. Am. J.*, 2013, **77**, 1996–2003.
23 A. R. Wadhawan, A. T. Stone and E. J. Bouwer, Biogeochemical controls on hexavalent chromium formation in estuarine sediments, *Environ. Sci. Technol.*, 2013, **47**, 8220–8228.
24 S. E. Fendorf and R. J. Zasoski, Chromium(III) oxidation by δ-manganese oxide (MnO_2). 1. Characterization, *Environ. Sci. Technol.*, 1992, **26**, 79–85.
25 E. L. Eary and D. Rai, Kinetics of chromium(III) oxidation to chromium(VI) by reaction with manganese dioxide, *Environ. Sci. Technol.*, 1987, **21**, 1187–1193.
26 R. Dai, J. Liu, C. Yu, R. Sun, Y. Lan and J. D. Mao, A comparative study of oxidation of Cr(III) in aqueous ions, complex ions and insoluble compounds by manganese-bearing mineral (birnessite), *Chemosphere*, 2009, **76**, 536–541.
27 Y. Tang, S. M. Webb, E. R. Estes and C. M. Hansel, Chromium(III) oxidation by biogenic manganese oxides with varying structural ripening, *Environ. Sci.: Processes Impacts*, 2014, **16**, 2127–2136.
28 D. Banerjee and H. W. Nesbitt, Oxidation of aqueous Cr(III) at birnessite surfaces: constraints on reaction mechanism, *Geochim. Cosmochim. Acta*, 1999, **63**, 1671–1687.
29 G. Landrot, M. Ginder-Vogel, K. Livi, J. P. Fitts and D. L. Sparks, Chromium(III) Oxidation by Three Poorly-Crystalline Manganese(IV) Oxides. 1. Chromium(III)-Oxidizing Capacity, *Environ. Sci. Technol.*, 2012, **46**, 11594–11600.

 This journal is © The Royal Society of Chemistry 2022

30 G. Landrot, M. Ginder-Vogel, K. Livi, J. P. Fitts and D. L. Sparks, Chromium(III) Oxidation by Three Poorly Crystalline Manganese(IV) Oxides. 2. Solid Phase Analyses, *Environ. Sci. Technol.*, 2012, **46**, 11601–11609.

31 G. Landrot, M. Ginder-Vogel and D. L. Sparks, Kinetics of Chromium(III) Oxidation by Manganese(IV) Oxides Using Quick Scanning X-ray Absorption Fine Structure Spectroscopy (Q-XAFS), *Environ. Sci. Technol.*, 2010, **44**, 143–149.

32 C. A. Johnson and A. G. Xyla, The oxidation of chromium (III) to chromium (VI) on the surface of manganite (γ-MnOOH), *Geochim. Cosmochim. Acta*, 1991, **55**, 2861–2866.

33 A. Manceau and L. Charlet, X-ray absorption spectroscopic study of the sorption of Cr(III) at the oxide-water interface, *J. Colloid Interface Sci.*, 1992, **148**, 425–442.

34 K. J. Murray and B. M. Tebo, Cr(III) Is Indirectly Oxidized by the Mn(II)-Oxidizing Bacterium Bacillus sp. Strain SG-1, *Environ. Sci. Technol.*, 2007, **41**, 528–533.

35 S. Namgung, M. Kwon, N. P. Qafoku and G. Lee, $Cr(OH)_3(s)$ oxidation induced by surface catalyzed Mn(II) oxidation, *Environ. Sci. Technol.*, 2014, **48**, 10760–10768.

36 P. S. Nico and R. J. Zasoski, Importance of Mn(III) Availability on the Rate of Cr(III) Oxidation on δ-MnO_2, *Environ. Sci. Technol.*, 2000, **34**, 3363–3367.

37 R. M. Weaver and M. F. Hochella, The reactivity of seven Mn-oxides with Cr 3+ aq: A comparative analysis of a complex, environmentally important redox reaction, *Am. Mineral.*, 2003, **88**, 2016–2027.

38 R. M. Weaver, M. F. Hochella and E. S. Ilton, Dynamic processes occurring at the CrIIIaq-manganite (γ-MnOOH) interface: simultaneous adsorption, microprecipitation, oxidation/reduction, and dissolution, *Geochim. Cosmochim. Acta*, 2002, **66**, 4119–4132.

39 W.-C. Wu, S.-L. Wang, Y.-M. Tzou, J.-H. Chen and M.-K. Wang, The adsorption and catalytic transformations of chromium on Mn substituted goethite, *Appl. Catal., B*, 2007, **75**, 272–280.

40 E. C. Butler, L. Chen, C. M. Hansel, L. R. Krumholz, A. S. E. Madden and Y. Lan, Biological versus mineralogical chromium reduction: potential for reoxidation by manganese oxide, *Environ. Sci.: Processes Impacts*, 2015, **17**, 1930–1940.

41 X. H. Feng, L. M. Zhai, W. F. Tan, W. Zhao, F. Liu and J. Z. He, The controlling effect of pH on oxidation of Cr(III) by manganese oxide minerals, *J. Colloid Interface Sci.*, 2006, **298**, 258–266.

42 N. Kozuh, J. Stupar and B. Gorenc, Reduction and oxidation processes of chromium in soils, *Environ. Sci. Technol.*, 2000, **34**, 112–119.

43 H. Guo, Y. Chen, H. Hu, K. Zhao, H. Li, S. Yan, W. Xiu, R. M. Coyte and A. Vengosh, High Hexavalent Chromium Concentration in Groundwater from a Deep Aquifer in the Baiyangdian Basin of the North China Plain, *Environ. Sci. Technol.*, 2020, **54**, 10068–10077.

44 D. L. Parkhurst, S. C. Christenson and G. N. Breit, *Ground-water-quality assessment of the central Oklahoma aquifer, Oklahoma—geochemical and geohydrologic investigations*, U.S. Geological Survey Water Supply Paper 2357-C, Reston, VA, 1996.

45 S. C. Christenson and J. S. Havens, *Ground-water-quality assessment of the central Oklahoma aquifer, Oklahoma: results of investigations*, U.S. Geological Survey Water Supply Paper 2357-A, 1998.

46 J. L. Schlottmann and R. A. Funkhouser, *Chemical analysis of water samples and geophysical logs from cored test holes drilled in the central Oklahoma aquifer, Oklahoma*, U.S. Geological Survey Open-File Report 91-464, Oklahoma City, OK, 1991.

47 J. Smith, S. Paxton, S. Christenson, R. Puls and J. Greer, *Flow Contribution and Water Quality with Depth in a Test Hole and Public-supply Wells: Implications for Arsenic Remediation Through Well Modification, Norman, Oklahoma, 2003-2006*, U.S. Environmental Protection Agency, Office of Research and Development, National Risk Management Laboratory, 2009.

48 R. Sutton, *Chromium-6 in US tap water*, Environmental Working Group, 2010.

49 G. N. Breit, C. A. Rice, K. J. Esposito and J. L. Schlottmann, *Mineralogy and petrography of Permian rocks in the central Oklahoma aquifer*, U.S. Geological Survey. Open-File Report 90-678, 1990.

50 G. N. Breit, *The diagenetic history of Permian rocks in the central Oklahoma aquifer, ground-water-quality assessment of the central Oklahoma aquifer, Oklahoma-results of investigations*, US Geological Survey Water-Supply Paper, 1998, pp. 45–70.

51 C. Becker, *Comparison of ground-water quality in samples from selected shallow and deep wells in the central Oklahoma aquifer, 2003-2005*, U.S. Geological Survey Scientific Investigations Report 2006-5084, 2006.

52 E. L. Mosier, C. S. Papp, J. M. Motooka, K. R. Kennedy and G. O. Riddle, *Sequential extraction analyses of drill core samples, central Oklahoma Aquifer*, U.S. Geological Survey Open-File Report 91-347, 1991.

53 R. J. Bartlett and B. R. James, Redox Chemistry of Soils, *Advances in Agronomy*, 1993, vol. 50, pp. 151–208.

54 A. Neaman, B. Waller, F. Mouélé, F. Trolard and G. Bourrié, Improved methods for selective dissolution of manganese oxides from soils and rocks, *Eur. J. Soil Sci.*, 2004, **55**, 47–54.

55 J. M. Asikainen and N. P. Nikolaidis, Sequential Extraction of Chromium from Contaminated Aquifer Sediments, *Groundwater Monit. Rem.*, 1994, **14**, 185–191.

56 A. L. Swindle, I. M. Cozzarelli and A. S. Madden, Using Chromate to Investigate the Impact of Natural Organics on the Surface Reactivity of Nanoparticulate Magnetite, *Environ. Sci. Technol.*, 2015, **49**, 2156–2162.

57 S. J. Smith and S. Christenson, *Naturally Occurring Arsenic in Ground Water, Norman, Oklahoma, 2004, and Remediation Options for Produced Water*, Report 2005-3111, 2005.

58 G. Sposito, C. Jouany, K. M. Holtzclaw and C. S. LeVesque, Calcium-Magnesium Exchange on Wyoming Bentonite in the Presence of Adsorbed Sodium, *Soil Sci. Soc. Am. J.*, 1983, **47**, 1081–1085.

59 G. Sposito, Effect of Chloride Ions on Sodium-Calcium and Sodium-Magnesium Exchange on Montmorillonite, *Soil Sci. Soc. Am. J.*, 1991, **55**, 965–967.
60 L. McNeill, J. McLean, M. Edwards and J. Parks, *State of the Science of Hexavalent Chromium in Drinking Water*, Water Research Foundation, 2012.
61 D. Diem and W. Stumm, Is dissolved Mn^{2+} being oxidized by O_2 in absence of Mn-bacteria or surface catalysts?, *Geochim. Cosmochim. Acta*, 1984, **48**, 1571–1573.
62 D. Fandeur, F. Juillot, G. Morin, L. Olivi, A. Cognigni, S. Webb, J.-P. Ambrosi, E. Fritsch, F. Guyot and G. Brown Jr, XANES Evidence for Oxidation of Cr(III) to Cr(VI) by Mn-Oxides in a Lateritic Regolith Developed on Serpentinized Ultramafic Rocks of New Caledonia, *Environ. Sci. Technol.*, 2009, **43**, 7384–7390.
63 A. Gonzalez, K. Ndung'u and A. Flegal, Natural Occurrence of Hexavalent Chromium in the Aromas Red Sands Aquifer, California, *Environ. Sci. Technol.*, 2005, **39**, 5505–5511.
64 K. Ndung'u, S. Friedrich, A. R. Gonzalez and A. R. Flegal, Chromium oxidation by manganese (hydr)oxides in a California aquifer, *Appl. Geochem.*, 2010, **25**, 377–381.
65 R. Bartlett and B. James, Studying dried, stored soil samples—some pitfalls, *Soil Sci. Soc. Am. J.*, 1980, **44**, 721.
66 A. J. Frierdich and J. G. Catalano, Fe(II)-Mediated Reduction and Repartitioning of Structurally Incorporated Cu, Co, and Mn in Iron Oxides, *Environ. Sci. Technol.*, 2012, **46**, 11070–11077.
67 A. J. Frierdich and J. G. Catalano, Controls on Fe(II)-Activated Trace Element Release from Goethite and Hematite, *Environ. Sci. Technol.*, 2012, **46**, 1519–1526.
68 A. J. Frierdich, M. M. Scherer, J. E. Bachman, M. H. Engelhard, B. W. Rapponotti and J. G. Catalano, Inhibition of Trace Element Release During Fe(II)-Activated Recrystallization of Al-, Cr-, and Sn-Substituted Goethite and Hematite, *Environ. Sci. Technol.*, 2012, 120906161352001, DOI: **10.1021/es302137d**, PMID – 22924460.
69 J. P. Westrop, MS thesis, University of Oklahoma, 2015.
70 J. E. Amonette and D. Rai, Identification of Noncrystalline $(Fe,Cr)(OH)_3$ by Infrared Spectroscopy, *Clays Clay Miner.*, 1990, **38**, 129–136.
71 C. Dai, X. Zuo, B. Cao and Y. Hu, Homogeneous and Heterogeneous $(Fex, Cr_{1-x})(OH)_3$ Precipitation: Implications for Cr Sequestration, *Environ. Sci. Technol.*, 2016, **50**, 1741–1749.
72 D. Rai, L. E. Eary and J. M. Zachara, Environmental chemistry of chromium, *Sci. Total Environ.*, 1989, **86**, 15–23.
73 F. Bloetscher, C. H. Sham, J. J. D. Ill and S. Ratick, Lessons Learned from Aquifer Storage and Recovery (ASR) Systems in the United States, *J. Water Resour. Prot.*, 2014, **06**, 1603–1629.
74 J. N. Weber, Trace element composition of dolostones and dolomites and its bearing on the dolomite problem, *Geochim. Cosmochim. Acta*, 1964, **28**, 1817–1868.
75 J. E. Johnson, S. M. Webb, C. Ma and W. W. Fischer, Manganese mineralogy and diagenesis in the sedimentary rock record, *Geochim. Cosmochim. Acta*, 2016, **173**, 210–231.

 This journal is © The Royal Society of Chemistry 2022